Supporting Information

Chang et al. 10.1073/pnas.1303002110

Analytical LC-MS Chromatogram and Mass Spectral Data of Stapled Peptides

The analytical liquid chromatography-mass spectrometry (LC-MS) chromatogram and mass spectral data of ATSP-7041 and its fluorescently-labeled analog (FAM-ATSP-7041) as well as the mass spectral data for each of the stapled peptides tested in this study provided confirmation of purity and structural integrity (Fig. S1, Table S1, and Table S2). The structural integrity of the pure products was analyzed by LC-MS using a SQ Detector interfaced with Waters Acquity UPLC system). The analytical LC-MS equipment and conditions for analysis of peptide products are given in Table S1. Representative LC chromatogram and mass spectrum of ATSP-7041 and FAM-ATSP-7041 are shown in Fig. S1, and the mass spectral data for each stapled peptide tested in this study are shown in Table S2.

Statistics from Data Collection and Structure Refinement of ATSP-7041 Complexed with MDMX

Details of the data collection and structure refinement are given in Table S3.

Topochemical Property Analysis from Molecular Modeling Studies and Investigation of the Staple Moiety in the Binding of ATSP-7041 to MDMX

A more detailed analysis of the comparative conformational properties of ATSP-7041 and related peptides complexed with MDM2 or MDMX is provided (Figs. S2 and S3) to further understand the impact of the staple moiety on the target protein binding. Specifically, we performed a detailed comparison of the stapled peptide structure to a linear peptide structure (PDB ID code 2z5t) from Popowicz et al. (1). Fig. S2 shows an overlay in two orientations of the two structures, and the correspondence of the two MDMX structures is readily evident (Fig. S2*A*). For the overlay, all Cα positions from the two target proteins (not the peptides) were used if their difference was less than 1 Å. The rmsd for the fit of the two proteins is 0.25 Å (based on 85/90 pairings). Examination of the two peptide structures in this overlay (Fig. S2*B*) shows a very good correspondence for their N-terminal half. However, at position 25 (Leu in 2z5t and Gln in the stapled peptide), the unstapled peptide starts to deviate from the canonical α-helical structure whereas ATSP-7041 maintains the α-helical to the C terminus. Despite this difference, the two residues that occupy the Leu pocket (Leu^{26} in 2z5t and Cba^{26} in the stapled peptide structure) are able to essentially fill the same space. At the N-terminal portions of each peptide, there is no significant shift of the stapled peptide up or down the α-helix axis (Fig. S2*B*). Similarly, the view down the α-helix axis (Fig. S2*C*) shows little or no twist around the α-helix axis for the stapled peptide relative to the peptide in the 2z5t structure. From this same view, the most apparent difference is a translational shift of about 0.4 Å of the stapled peptide closer to MDMX. This observation is interesting in that the structure of SAH-p53-8 with MDM2(37) shows a shift along the α-helix axis of about 1 Å in the N-terminal direction and a rotation of about 18° around the helix axis. Nevertheless, this finding may or may not represent an important difference between ATSP-7041 and SAH-p53-8. An overlay of those two structures (Fig. S3) shows the well-described differences between the MDM2 and MDMX structures, but the two stapled peptides match up exceedingly well, with the minor exception of the extreme C termini (Fig. S3).

Plasma Protein (Albumin) Binding Properties of ATSP-7041 and ATSP-3900 Using Ultracentrifugation

ATSP-7041 and ATSP-3900 stock solutions (10 mM in DMSO) were spiked into 1 mL of human plasma, obtaining the final sample with ~2 μM peptides. The samples were centrifuged at 200,000 × *g* for 22 h at 25 °C. The total drug concentrations (in plasma samples before centrifugation) and free drug concentrations (in the protein-free supernatant after centrifugation) were measured by LC-MS. The percentages of unbound were calculated. Similarly, plasma protein binding in monkey, dog, rat, and mouse was also measured for ATSP-7041. In summary, it was determined that both ATSP-7041 and ATSP-3900 were highly complexed to human albumin (98.2% and 97.2% fraction bound, respectively) and that such findings were comparable for ATSP-7041 relative to monkey, dog, rat, and mouse albumins (Table S4).

ATSP-7041 Exhibits Favorable DMPK and Tissue Distribution Properties

The calculated PK parameters for extravascular tissues in Table S5 indicate that [^{3}H]-ATSP-7041 distributes extensively throughout the body with the exception of brain and CNS tissues, which was limited, as was erythrocyte penetrance. Highly vascularized tissues, including essential target tissues for the treatment of solid and hematologic tumors, showed the greatest tissue-to-plasma $AUC_{0\text{-}t}$ ratios, including the lymph node (1.0), liver (0.6), small intestinal wall (0.6), lung (0.5), adrenal gland (0.5), spleen (0.4), bone marrow (0.3), large intestine wall (0.3), pancreas (0.2), pituitary gland (0.2), and thyroid gland (0.2).

Quantitative whole-body autoradiography images indicate that the radiolabel appears in small intestine contents and, at later time points, lower GI contents, suggesting biliary clearance for this stapled peptide. To confirm this hypothesis, excreta and bile samples were evaluated in intact and biliary duct-cannulated (BDC) rats throughout a 48 h post dose period to determine route of elimination of i.v.-administered [^{3}H]-ATSP-7041. As shown in Table S6, the majority of the administered radioactive dose was eliminated in the bile after 48 h whereas less than 3% of the total dose was recovered in urine. [^{3}H]-ATSP-7041 was identified as the only circulating component in plasma, and only the unchanged parent compound was detected in the bile over several plasma half-lives of the parent compound. The total radioactivity recovered in feces and bile over the sampling interval in BDC rats (79%) was similar to that recovered in the feces of intact male rats (67%) over the same interval, indicating that enterohepatic recirculation does not play a role in the disposition of [^{3}H]-ATSP-7041.

1. Popowicz GM, et al. (2007) Molecular basis for the inhibition of p53 by Mdmx. *Cell Cycle* 6(19):2386–2392.

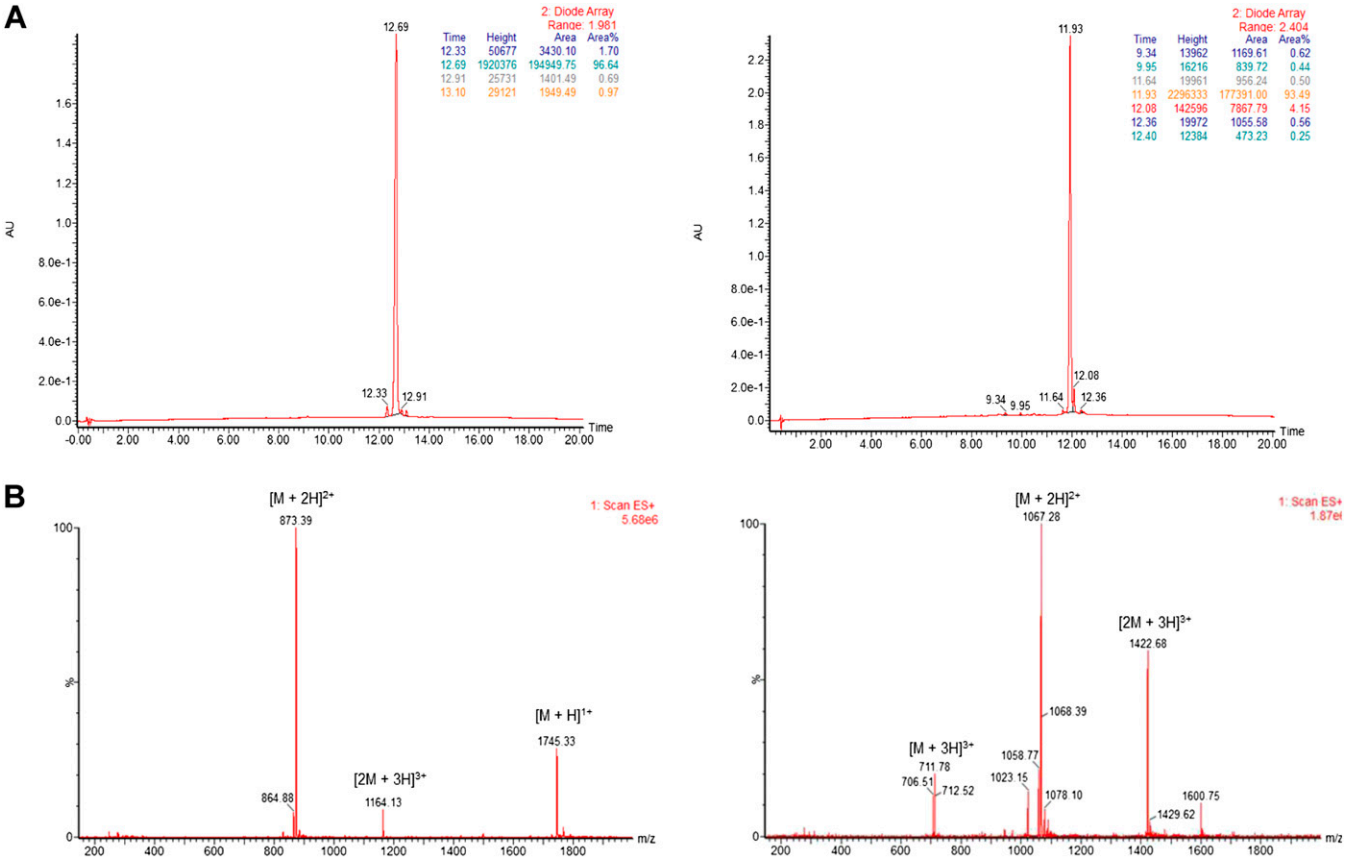

Fig. S1. Representative LC-MS traces from purified peptide ATSP-7041and its FAM-ATSP-7041. All LC-MS samples were run on a Waters Acquity UPLC system using a Phenomenex C8 column. (*A*) LC chromatogram of peptide ATSP-7041. (*B*) Electrospray mass spectrum (positive ion mode) of peptide ATSP-7041.

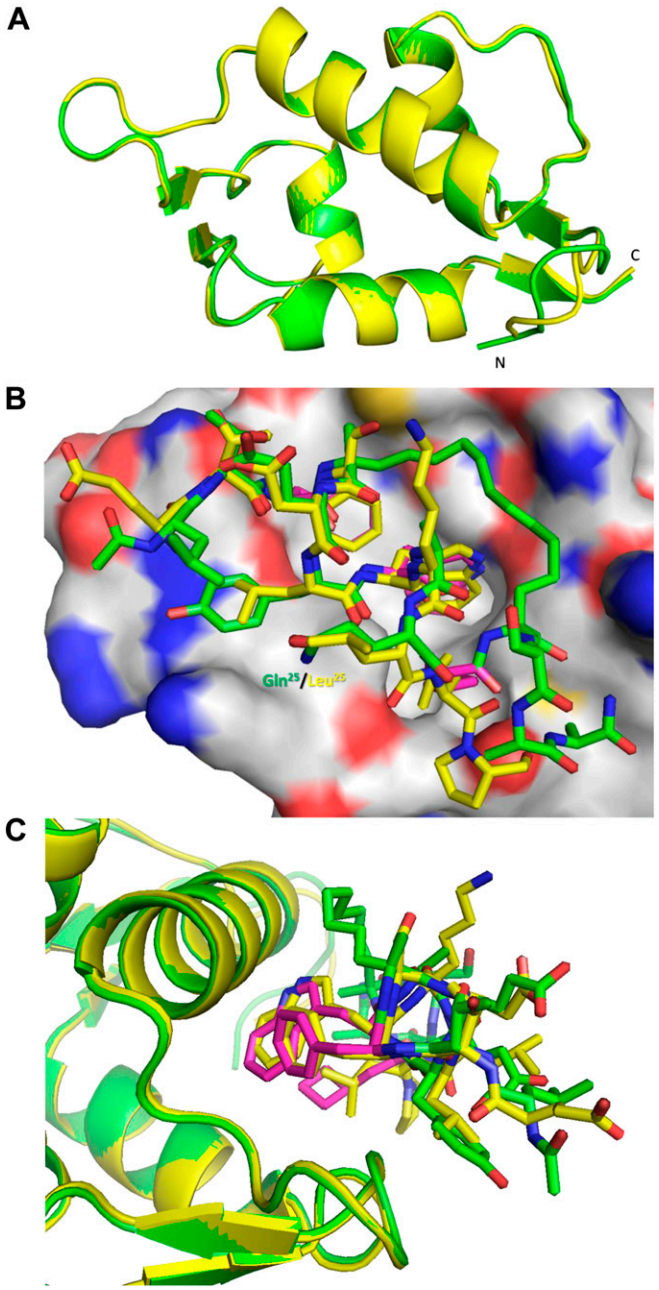

Fig. S2. Stapled peptide ATSP-7041 exhibits enhanced helicity compared with a linear peptide analog. (*A*) The superposition of the Ca backbones of MDMX bound with p53 (yellow) and MDMX bound to ATSP-7041 (green) show a very high structural similarity. (*B*) Further analysis of this superposition shows very similar binding of p53 (yellow) and ATSP-7041 (green) at their respective N-terminus, but at amino acid position 25 it is observed that p53 does not sustain α-helical integrity. (*C*) A comparative view of p53 and ATSP-7041 along their respective α-helical axis reveals highly similar conformational properties. The staple moiety as well as the key side chains (magenta) of ATSP-7041 show closer proximity of contact with MDMX protein relative to their equivalent residues from p53.

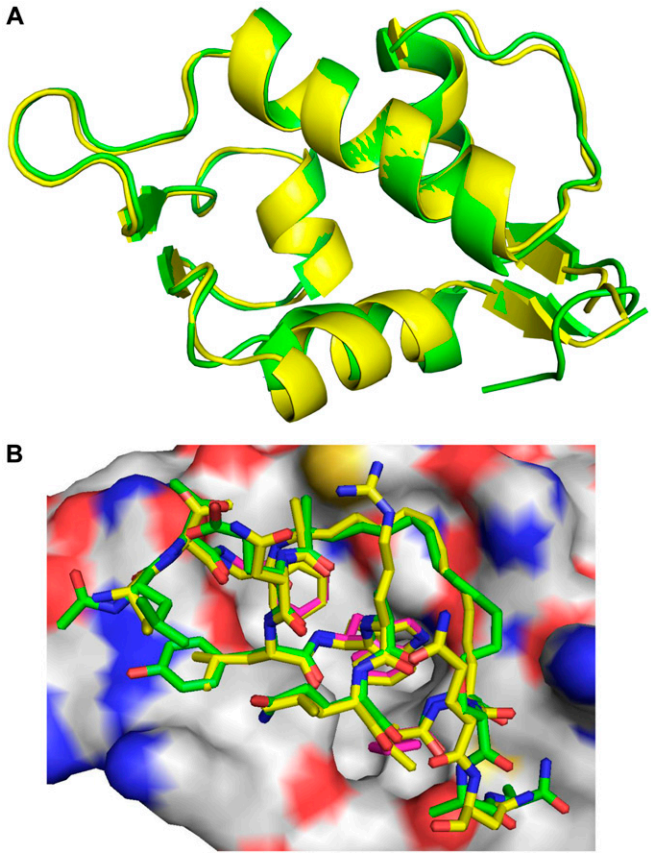

Fig. S3. Stapled peptide binding to MDMX is essentially equivalent with binding to MDM2. (*A*) An overlay of MDMX (green) and MDM2 (yellow) proteins show the well-described difference at helix α-2′. (*B*) An overlay in MDM2 protein bound with ATSP-7041 (green) and MDM2 bound with SAH-p53-8 show essentially identical binding interactions except at the C-terminal sequences of the two stapled peptides.

Table S1. Analytical LC-MS equipment and conditions for analysis

Parameter	Details
Column	Kinetex C18 2.1 × 100 mm (Phenomenex, 100Å pore size, 2.6 μm particle size)
Mobile phase	A: water, 0.1% trifluoroacetic acid; B: acetonitrile, 0.1% trifluoroacetic acid
Flow rate	0.6 mL/min
Gradient	20-80% B over 20 min
Injection volume	5 μL
Wavelength (nm)	214

Table S2. Mass spectral data for peptides tested in this study

Stapled peptide	Calculated [M + 2]/2	Found [M + 2]/2	Purity, %
ATSP-1800	1055.08	1055.44	93.7
ATSP-3848	768.88	769.23	87.9
ATSP-3900	799.94	800.31	91.5
ATSP-4641	766.93	767.38	94.7
ATSP-6935	795.93	796.33	93.3
ATSP-7041	872.97	873.39	96.6
ATSP-7342	834.95	835.27	96.1
FAM-ATSP-7041	1066.51	1067.28	93.5
FAM-mt-7041	1028.49	1029.44	93.1

Table S3. Statistics from data collection and structure refinement of ATSP-7041 complexed with MDMX

Parameter	Details
Data collection	
Space group	$C222_1$
Cell dimensions	
a, *b*, *c* (Å)	81.585, 108.535, 30.964
α, β, γ (°)	90.0, 90.0, 90.0
Resolution (Å)	1.64 (1.75-1.64)*
Rsym or *Rmerge*	0.042 (0.375)
$I/\sigma(I)$	9.3 (1.9)
Completeness (%)	99.8 (100)
Redundancy	6.4 (6.7)
Refinement	
Resolution (Å)	1.7
Number of reflections	15,537
R_{work}/R_{free}	0.210/0.224
Number of atoms	
Protein	724
Ligand	125
Water	119
B-factors	
Protein	31.96
Ligand	27.63
Water	43.25
Rms deviations	
Bond lengths (Å)	0.005
Bond angles (Å)	1.374

*Values in parentheses are results for the highest resolution shell.

Table S4. Plasma protein (albumin) binding properties of ATSP-7041 and ATSP-3900 using ultracentrifugation

	% Fraction of unbound				
Species	Mouse	Rat	Dog	Monkey	Human
ATSP-7041	7.7	3.1	5.3	2	2.8
ATSP-3900					1.8

Table S5. Estimated mean pharmacokinetic parameters of selected matrixes/tissues following i.v. administration of [^{3}H]-ATSP-7401 at 5 mg/kg to male Long–Evans rats

Tissue	C_{max} (ng equiv./g)*	Apparent $t_{½b}$ (hr)*	AUC_{0-24} (ng equiv.·hr/g)*	AUC_{0-inf} (ng equiv.·hr/g)*	Tissue: plasma**
Plasma	66258	13.6	253481	261163	1.0
Blood	30177	17.7	124911	133726	0.5
Lymph node	12252	NC	245374	NC	1.0
Liver	19515	19.1	160541	184725	0.6
Small Intestine Wall	15223	21.5	156289	NC	0.6
Lung	27451	18.9	128865	143186	0.5
Kidney	15710	28.6	118404	159562	0.5
Adrenal Gland	12505	63.9	117216	242715	0.5
Spleen	6143	28.4	105668	151331	0.4
Bone Marrow	6100	30.0	86421	122176	0.3
Large Intestine Wall	2866	25.2	82199	114428	0.3
Pituitary Gland	5293	68.3	61137	140810	0.2
Thyroid Gland	4295	30.6	53715	77750	0.2
Pancreas	3025	21.8	51243	67476	0.2
Brain	656	NC	4326	NC	0.0

NC, not calculable.
*ng equiv./g, equivalent ng levels of drug per gram tissue based on radiolabel quantification.
**Based on AUC0-24.

Table S6. Recovery of ^{3}H-ATSP-7401 in rat bile and excreta over 48 h post dose following i.v. administration of [^{3}H]-ATSP-7401 at 5 mg/kg

Animal ID	Bile	Urine	Feces	Cage rinse	Cage wash	Total
Intact-1	n/a	1.5	67.0	0.2	0.1	68.7
Intact-2	n/a	3.7	67.4	0.4	0.1	71.6
BDC-1	74.4	4.9	1.2	0.1	0.2	80.8
BDC-2	81.7	4.1	1.1	0.2	0.2	87.3

n/a, not applicable.